AIMETA '01
XV Congresso AIMETA di Meccanica Teorica e Applicata
15th AIMETA Congress of Theoretical and Applied Mechanics

A PU-FE APPROACH TO QUASI-BRITTLE FRACTURE

S. MARIANI*, U. PEREGO‡

Dipartimento di Ingegneria Strutturale, Politecnico di Milano
Piazza Leonardo da Vinci 32, 20133, Milano

e-mail: * mariani@stru.polimi.it, ‡ perego@stru.polimi.it

ABSTRACT

A new computational strategy for the simulation of crack growth processes in quasi-brittle materials is proposed; it is centered on the partition of unity (PU) concept, first presented by Babuška and coworkers in [1, 2]. The PU methodology, through an enrichment of the displacement field, allows a description of the displacement discontinuity, which is independent of the original mesh layout. This implies a high degree of flexibility in the definition of the crack pattern and propagation. Results for mode I cohesive crack growth in a model problem are presented to illustrate the potentiality of the proposed approach.

SOMMARIO

Si propone una nuova strategia computazionale per la simulazione della propagazione di una frattura in un materiale quasi-fragile, basata sul concetto della Partizione dell'Unità (PU) proposta per la prima volta da Babuška e dai suoi collaboratori in [1, 2]. Tramite un arricchimento del campo di spostamento, la metodologia PU consente di descrivere la discontinuità di spostamento in modo indipendente dalla mesh originale. Questa caratteristica porta ad una elevata flessibilità nella definizione del percorso della frattura. Per illustrare le potenzialità dell'approccio proposto, si presentano i risultati relativi alla propagazione in modo I di una cricca coesiva in un problema modello per un solido elastico lineare.

1 INTRODUCTION

For fracture processes in quasi-brittle materials the dissipative mechanisms are predominantly concentrated along cohesive fracture surfaces, while the material in the remaining background domain is often assumed as indefinitely linear elastic. The sources of nonlinearities are thus located only along lower-dimensionality loci, which require to be accurately discretized within a Finite Element (FE) context.

In recent years various alternative approaches to quasi-brittle fracture phenomena have been proposed. Among others, it is worth mentioning here: (a) the use of cohesive interface elements with explicit discretization of the fracture process zone either from a priori [3, 4], or just after crack activation [5]; (b) the use of embedded crack elements, which

model the crack evolution inside finite elements by means of discontinuous enhanced displacement fields [6, 7, 8, 9].

An alternative approach is followed herein inspired to the PU-FE method (also named generalized or extended FE method), recently presented by Babuška and coworkers. By exploiting the property for which the sum of the nodal shape functions, here defined with a compact support, is unit everywhere in the domain to be modeled, displacement finite element approximate solutions can be enhanced through the introduction of ad-hoc assumed local functions. In this way, local known features of the exact solution can be introduced into the standard FE approximation fields [10, 11].

So far, the PU-FE method has been primarily used to model the effects of reentrant corners in elastic domains [12] and crack processes in brittle materials [13, 14, 15]; for both problems the asymptotic elastic solutions in the vicinity of a corner or crack tip are known with the corresponding stress intensity factors.

The present contribution addresses two aspects of the formulation of PU-FEs for quasi-brittle fracture mechanics: cohesive forces between the two flanks of the opening crack in the process zone lead to a reduction of the stress concentration ahead of the tip of the process zone, so that the stress intensity factors of linear elastic fracture mechanics (and the relevant asymptotic solutions for displacements) are not correct for the considered problem; the simulation of crack growth requires not only a description of the discontinuous displacement field across the crack but also a particularly accurate modelling of the deformation state in the bulk of the solid, in proximity of the process zone, especially ahead of its tip. These two issues are here addressed by means of local enhancement of the displacement model for three-noded constant strain triangles; the local enhancement consists of quadratic polynomials, which are discontinuous across the fracture. This procedure allows to obtain PU-FE solutions with a cubic displacement modelling of the crack opening in the process zone, containing unknowns only in the vertex nodes of the original mesh, with the addition of only one node at each crack kink.

In order to emphasize the basic characteristic of the proposed method, only mode I cohesive fracture processes in two-dimensional linear elastic media under small displacements assumption are considered in this work.

2 GOVERNING EQUATIONS

Let us consider a three-dimensional domain Ω bounded by the two disjointed surfaces Γ_t and Γ_u (such that $\Gamma_t \cup \Gamma_u = \Gamma$ and $\Gamma_t \cap \Gamma_u = \emptyset$) on which tractions and displacements are imposed, respectively, and by a propagating internal fracture surface Γ_d (Figure 1). Γ_d consists of a crack surface on which the interaction between crack flanks is possible only upon crack closure under compressive stress states, and of the current fracture process zone, where cohesive interaction between the opening (and possibly sliding) surface flanks is taking place.

In what follows it is assumed that the crack originates from the boundary so that only one running crack tip has to be followed during crack growth; this is not a limitation of the proposed approach but allows to rule out bifurcation phenomena along the equilibrium path. Similarly, during the analyses possible crack branching phenomena are not accounted for.

The equilibrium of the quasi-brittle medium described above is governed by the fol-

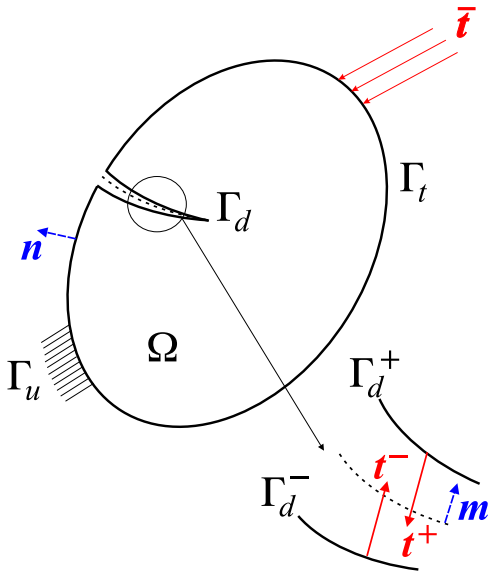

Figure 1: Geometry of modeled domain and notation.

lowing equations:

$$\boldsymbol{\mathcal{C}}^{\mathrm{T}}\boldsymbol{\sigma} + \bar{\boldsymbol{b}} = \boldsymbol{0} \qquad \text{in } \Omega; \tag{1}$$

$$\boldsymbol{\sigma}\boldsymbol{n} = \bar{\boldsymbol{t}} \qquad \text{on } \Gamma_t; \tag{2a}$$

$$\boldsymbol{\sigma}\boldsymbol{m} = -\boldsymbol{t}^+ \qquad \text{on } \Gamma_d^+, \qquad \boldsymbol{\sigma}\boldsymbol{m} = \boldsymbol{t}^- \qquad \text{on } \Gamma_d^-. \tag{2b}$$

Here: $\boldsymbol{\sigma}$ is the vector of stress components; $\bar{\boldsymbol{b}}$ and $\bar{\boldsymbol{t}}$ are the assigned external loads per unit volume and surface, respectively; $\boldsymbol{\mathcal{C}}$ is the differential compatibility operator; $\boldsymbol{n}$ is the unit outward normal to Γ and $\boldsymbol{m}$ is the unit normal to Γ_d, defined by the direction of propagation as shown in Figure 1; accordingly, Γ_d^+ and Γ_d^- define the two sides of the crack acted upon by tractions $\boldsymbol{t}^+$ and $\boldsymbol{t}^-$, which express the cohesive interaction in the fracture process zone. The equilibrium condition across the fracture surface Γ_d reads:

$$\boldsymbol{t} \doteq \boldsymbol{t}^- = -\boldsymbol{t}^+. \tag{3}$$

Under the assumption of linearized kinematics, the compatibility conditions in Ω and along Γ_u are given by

$$\boldsymbol{\varepsilon} = \boldsymbol{\mathcal{C}}\boldsymbol{u} \qquad \text{in } \Omega, \;\; \boldsymbol{u} = \bar{\boldsymbol{u}} \qquad \text{on } \Gamma_u; \tag{4}$$

$\boldsymbol{\varepsilon}$ and $\boldsymbol{u}$ being the strain and the displacement vectors, respectively, and $\bar{\boldsymbol{u}}$ the assigned values of displacements along Γ_u.

The material behavior is assumed linear elastic for the bulk material in Ω, i.e.

$$\boldsymbol{\sigma} = \boldsymbol{D}\boldsymbol{\varepsilon} \qquad \text{in } \Omega, \tag{5}$$

while a nonlinear elastic-softening (holonomic) interface behavior is assumed on Γ_d (Figure 2), described by:

$$\boldsymbol{t} = \begin{cases} \boldsymbol{E}_d\,[\boldsymbol{u}] + \big\langle\, [\boldsymbol{u}] - [\boldsymbol{u}]_M \,\big\rangle(\boldsymbol{Q}_d - \boldsymbol{E}_d) & \text{if } [\boldsymbol{u}] \le [\boldsymbol{u}]_u \\ \boldsymbol{0} & \text{if } [\boldsymbol{u}] > [\boldsymbol{u}]_u \end{cases} \qquad \text{on } \Gamma_d. \tag{6}$$

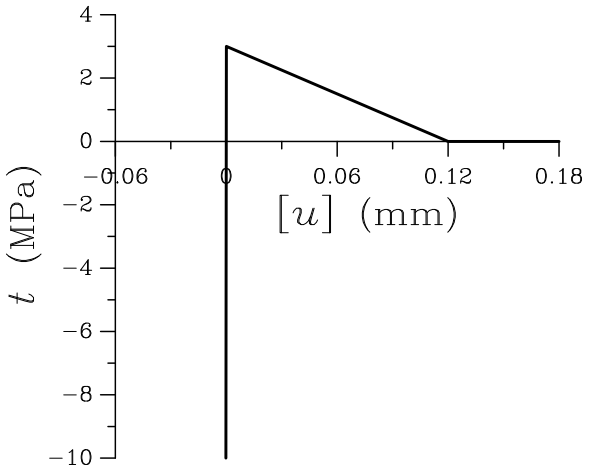

Figure 2: Mode I assumed constitutive behavior in the process zone.

In (5) and (6) $\boldsymbol{D}$ is the matrix of elastic moduli; $\boldsymbol{E}_d$ and $\boldsymbol{Q}_d$ are the positive and negative elastic stiffnesses, respectively, of the two linear branches of the interface traction-displacement discontinuity curve ; $[\boldsymbol{u}]$ denotes the displacement discontinuity along Γ_d, defined as:

$$[\boldsymbol{u}] = \boldsymbol{u}\Big|_{\Gamma_d^+} - \boldsymbol{u}\Big|_{\Gamma_d^-} . \tag{7}$$

The two terms at the right-hand side represent the displacement field computed on Γ_d^+ and Γ_d^-, respectively; $[\boldsymbol{u}]_M$ and $[\boldsymbol{u}]_u$ in (6) indicate the displacement discontinuity at the peak and at vanishing cohesive tractions (see Figure 2 for mode I loadings); the symbol $\langle\ \rangle$ denotes the McAuley brackets ($\langle x \rangle = 1/2(x + |x|)$).

The traction-displacement discontinuity relationship along Γ_d is concisely expressed in rate form by:

$$\dot{\boldsymbol{t}} = \boldsymbol{D}_\Gamma^t \, [\dot{\boldsymbol{u}}] \, , \tag{8}$$

$\boldsymbol{D}_\Gamma^t$ being the matrix of interface tangent moduli ($\boldsymbol{D}_\Gamma^t = \boldsymbol{E}_d$ for $[\boldsymbol{u}] \leq [\boldsymbol{u}]_M$, $\boldsymbol{D}_\Gamma^t = \boldsymbol{Q}_d$ for $[\boldsymbol{u}]_M < [\boldsymbol{u}] \leq [\boldsymbol{u}]_u$, $\boldsymbol{D}_\Gamma^t = \boldsymbol{0}$ for $[\boldsymbol{u}]_u < [\boldsymbol{u}]$). More advanced interface laws are discussed e.g. in [16].

3 FINITE ELEMENT FORMULATION

Let $\mathcal{U}$ be the space of admissible displacements $\boldsymbol{u}$ in Ω, i.e. such that $\boldsymbol{u} = \bar{\boldsymbol{u}}$ on Γ_u, $\boldsymbol{u}$ possibly discontinuous on Γ_d and $\boldsymbol{u} \in C^0$ everywhere else in Ω. By introducing the test functions $\boldsymbol{v} \in \mathcal{U}_0$ (with zero prescribed displacements on Γ_u), the weak form of the incremental equilibrium equations reads:

$$\int_{\Omega} \boldsymbol{\varepsilon}^{\mathrm{T}}(\boldsymbol{v})\,\dot{\boldsymbol{\sigma}}\,d\Omega = \int_{\Omega} \boldsymbol{v}^{\mathrm{T}}\dot{\bar{\boldsymbol{b}}}\,d\Omega + \int_{\Gamma_t} \boldsymbol{v}^{\mathrm{T}}\dot{\bar{\boldsymbol{t}}}\,d\Gamma_t + \int_{\Gamma_d^+} \boldsymbol{v}^{\mathrm{T}}\dot{\boldsymbol{t}}^{+}\,d\Gamma_d + \int_{\Gamma_d^-} \boldsymbol{v}^{\mathrm{T}}\dot{\boldsymbol{t}}^{-}\,d\Gamma_d$$
$$= \int_{\Omega} \boldsymbol{v}^{\mathrm{T}}\dot{\bar{\boldsymbol{b}}}\,d\Omega + \int_{\Gamma_t} \boldsymbol{v}^{\mathrm{T}}\dot{\bar{\boldsymbol{t}}}\,d\Gamma_t - \int_{\Gamma_d} [\boldsymbol{v}]^{\mathrm{T}}\,\dot{\boldsymbol{t}}\,d\Gamma_d \qquad \forall \boldsymbol{v} \in \mathcal{U}_0. \tag{9}$$

In equation (9) use has been made of the fact that, in view of the assumed linearized kinematics, $\Gamma_d \equiv \Gamma_d^+ \equiv \Gamma_d^-$.

Taking into account the constitutive laws for the bulk material (5) and for the cohesive part (6) of the fracture surface, the structural problem can be expressed in variational form as:

$$\begin{aligned} \text{find } \dot{\boldsymbol{u}} \in \mathcal{U}: \quad & \int_{\Omega} \boldsymbol{\varepsilon}^{\mathrm{T}}(\boldsymbol{v})\,\boldsymbol{D}\dot{\boldsymbol{\varepsilon}}(\dot{\boldsymbol{u}})\,d\Omega + \int_{\Gamma_d} [\boldsymbol{v}]^{\mathrm{T}}\,\boldsymbol{D}_{\Gamma}^{t}\,[\dot{\boldsymbol{u}}]\,d\Gamma_d \\ & = \int_{\Omega} \boldsymbol{v}^{\mathrm{T}}\dot{\bar{\boldsymbol{b}}}\,d\Omega + \int_{\Gamma_t} \boldsymbol{v}^{\mathrm{T}}\dot{\bar{\boldsymbol{t}}}\,d\Gamma_t \quad \forall \boldsymbol{v} \in \mathcal{U}_0. \end{aligned} \tag{10}$$

Since we confine our attention to two-dimensional domains, the fracture surface Γ_d reduces to a line within Ω. The approximate PU-FE solution is obtained subdividing first the domain Ω into a standard mesh of triangular finite elements. The discretized displacement field $\boldsymbol{u}^h(\boldsymbol{x})$ is then obtained according to the following *enriched* model:

$$\boldsymbol{u}^h(\boldsymbol{x}) = \sum_{i \in I} \phi_i(\boldsymbol{x})\,\boldsymbol{u}^i + \sum_{j \in J} \sum_{k=0}^{3} \mathcal{H}(\boldsymbol{x})\,\phi_j(\boldsymbol{x})\,\psi_{kj}(\boldsymbol{x})\,{}^k\boldsymbol{\delta}^j, \tag{11}$$

where set I collects all the nodes of the triangulation, while set J gathers only those nodes, except for the current tip node, whose support ω_j is cut by Γ_d. $\phi_i(\boldsymbol{x})$ is the usual linear shape function centered at node i (according to the notation used in [2], $\phi_i(\boldsymbol{x})$ is the *partition of unity* subordinate to the covering $\{\omega_i\}$ of domain Ω); $\mathcal{H}(\boldsymbol{x})$ is the Heaviside step-function, defined as:

$$\mathcal{H}(\boldsymbol{x}) = \begin{cases} +1 & \text{if } (\boldsymbol{x} - \boldsymbol{x}^*)^{\mathrm{T}}\,\boldsymbol{m} > 0 \\ -1 & \text{if } (\boldsymbol{x} - \boldsymbol{x}^*)^{\mathrm{T}}\,\boldsymbol{m} < 0 \end{cases} \tag{12}$$

$\boldsymbol{x}^*$ being the closest point projection of $\boldsymbol{x}$ onto Γ_d. $\psi_{kj}(\boldsymbol{x})$ $(k = 0, 1, 2, 3)$ are the enrichment functions, here defined as:

$$\psi_{0j}(\boldsymbol{x}) = 1, \tag{13}$$

$$\psi_{1j}(\boldsymbol{x}) = \left(\frac{x - x_j}{h_j}\right)^2, \tag{14}$$

$$\psi_{2j}(\boldsymbol{x}) = \left(\frac{y - y_j}{h_j}\right)^2, \tag{15}$$

$$\psi_{3j}(\boldsymbol{x}) = \left(\frac{x - x_j}{h_j}\right)\left(\frac{y - y_j}{h_j}\right). \tag{16}$$

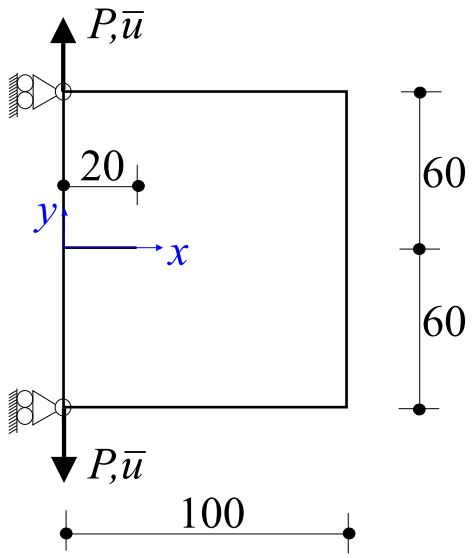

Figure 3: Specimen geometry and applied boundary conditions (mm).

h_j is a scaling factor introduced to reduce pollution errors in the numerical solution and is related to the mean size of the elements that are currently sharing the vertex node j (in the example shown in the forthcoming Section it has been set $h_j = 1$); $\boldsymbol{u}^i$ are the standard nodal degrees of freedom which represent the values of displacements for $\boldsymbol{x} \equiv \boldsymbol{x}_i$, when $i \notin J$; ${}^k\boldsymbol{\delta}^j$ are the additional nodal degrees of freedom introduced in order to enhance the displacement model.

The proposed approximation (11) is able to capture accurately two of the main features of the exact solution, i.e.:

- the discretized displacement field is discontinuous across Γ_d, thanks to the presence of $\mathcal{H}(\boldsymbol{x})$ in the enhanced term of the assumed displacement model $\boldsymbol{u}^h(\boldsymbol{x})$, with discontinuity given by

$$[\boldsymbol{u}]^h = \boldsymbol{u}^h\Big|_{\Gamma_d^+} - \boldsymbol{u}^h\Big|_{\Gamma_d^-} = \sum_{j\in J}\sum_{k=0}^{3} 2\Big(\phi_j(\boldsymbol{x})\,\psi_{kj}(\boldsymbol{x})\Big)_{\Gamma_d}\,{}^k\boldsymbol{\delta}^j; \tag{17}$$

- the opening displacement along Γ_d displays a cusp-like shape in the process zone, where cohesive tractions have the effect to eliminate the stress singularity ahead of the crack tip, typical of linear elastic fracture mechanics.

A major drawback of the proposed solution is that the enhanced displacement interpolation lead to a semidefinite matrix of tangent stiffness moduli. However, the spurious zero energy modes do not correspond to any deformation of the element, which therefore passes the patch test. In this work, results have been obtained by solving iteratively the linearized system of equations, according to the technique proposed in [12].

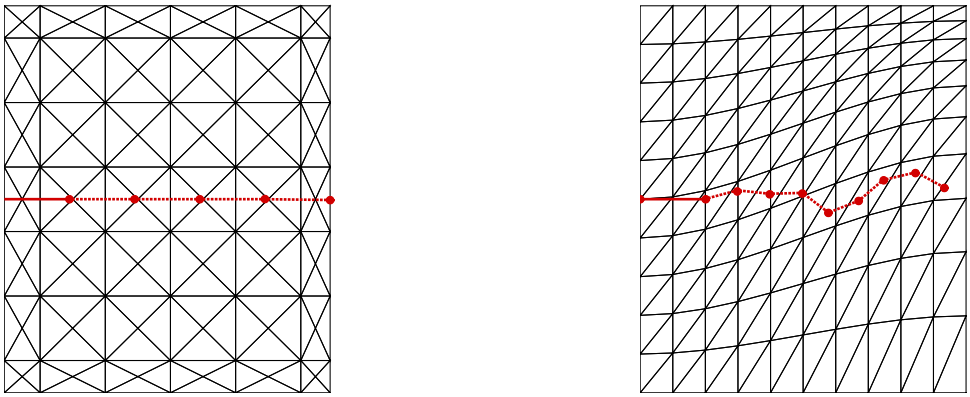

(a) (b)

Figure 4: (a) Symmetric and (b) biased meshes used to discretize the model problem

4 MODE I CRACK GROWTH IN A MODEL PROBLEM

The proposed PU-FE approach is used to analyze the crack growth in the thin pre-notched specimen shown in Figure 3. Due to the symmetry of geometry and applied boundary conditions, a rectilinear mode I crack growth is expected.

Material properties are set as: bulk material (in Ω): Young's modulus $E = 20000$ (MPa), Poisson's ratio $\nu = 0.2$; mode I cohesive interface (on Γ_d): first branch elastic stiffness $E_d = 50000$ (MPa/mm), second branch elastic stiffness $Q_d = -25$ (MPa/mm), maximum traction carrying capacity $t_{1M} = 3$ (MPa). Figure 2 shows the assumed mode I, traction $t_{\rm I}$ vs opening displacement $[u_{\rm I}]$, law (subscript I is dropped for brevity in the remainder of this Section); the mode II, $t_{\rm II} - [u_{\rm II}]$ behavior is instead assumed indefinitely linear elastic. According to these model parameters, the mode I fracture toughness is $G_{\rm I} = 0.18$ (N/mm).

Figure 4 shows the two discretizations used: (a) has a layout symmetric with respect to the expected propagation path; (b) is biased in order to introduce a preferential, spurious inclined layout. In the figure the dots represent the position of crack tip at each stage of the computed fracture propagation. The continuous solid lines denote the initial pre-notch while the dotted straight segments that connect the dots represent the evolution of Γ_d under the applied loading conditions.

The adopted fracture growth criterion allows a step-wise propagation of Γ_d when the maximum tensile stress ahead of the tip of the process zone is greater that t_{1M}. The local direction of fracture propagation is assumed orthogonal to the direction of the maximum tensile stress. In Figure 4 it can be seen that, due to round-off errors and lack of symmetry in the biased mesh, Γ_d does propagate following a zig-zag polyline path around the rectilinear propagation direction. For comparison purposes, this specimen has been also modeled by means of 8-noded isoparametric element in Ω and by means of 6-noded interface elements with the cohesive constitutive law (6). In this case, only one half of

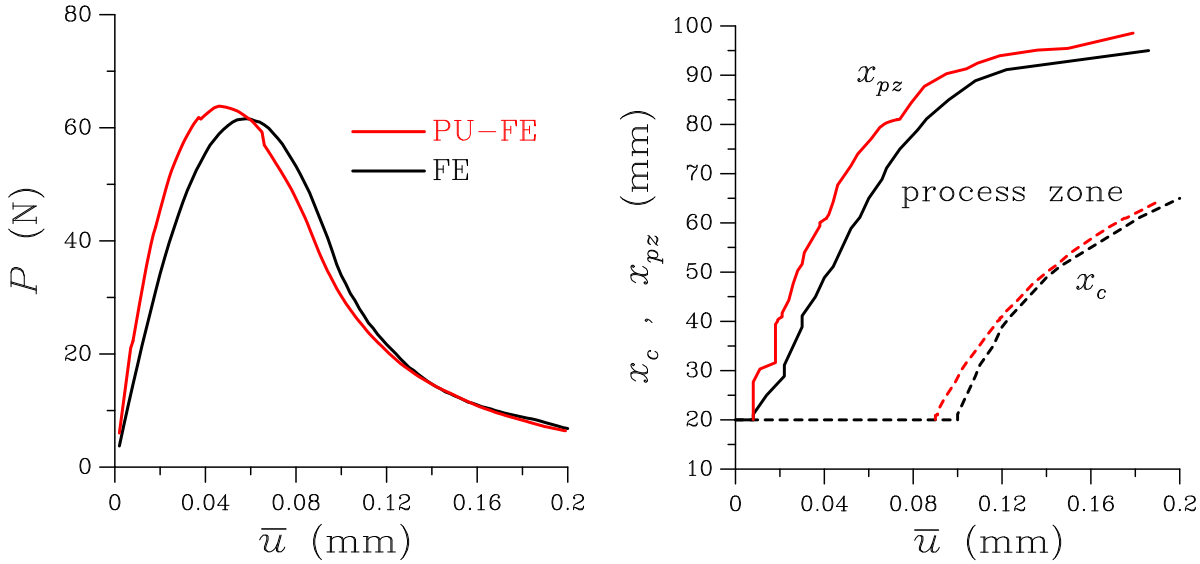

(a) (b)

Figure 5: (a) Measured load P vs imposed displacement $\bar{u}$ response of the specimen; (b) current position of crack tip (x_c) and fracture process zone tip (x_{pz}) for given displacement $\bar{u}$.

the specimen has been discretized due to symmetry conditions.

Figure 5a shows the computed reaction P vs imposed displacement $\bar{u}$ curve. In this and in the forthcoming figures, "FE" refers to the FE solution obtained with interface elements, while "PU-FE" refers to the solution obtained with the enhanced PU-FE approach and symmetric discretization. Even though the two approaches are based on different techniques for the simulation of the crack growth, the modeled global behavior is substantially the same. The main difference appears not to be related to the assumed crack propagation scheme but rather it concerns the initial elastic behavior, which is stiffer in the PU-FE simulation due to the coarse discretization of Ω. From Figure 5a one can also observe slight oscillations in the $P - \bar{u}$ PU-FE curve in correspondence of each tip advancement. This is mainly due to the finite size of the imposed increment of fracture length $\Delta a = 20$ (mm) adopted in the PU-FE simulation, which is defined a priori and is neither related to the actual crack length nor to the size of the fracture process zone. To compensate for the numerical sudden topology modification of Γ_d, a finite initial elastic stiffness has been introduced in the interface behavior (see equations 6). The oscillations could be further lowered just reducing the size of Δa. Figure 5b presents a comparison between the FE and PU-FE solutions concerning the positions of the tip (x_c) of the crack and the tip (x_{pz}) of the process zone ($x_{pz} - x_c$ being the length of the process zone) vs. the prescribed displacement $\bar{u}$. It can be noted that x_c evolves smoothly during the PU-FE analysis, while a slightly irregular behavior is observed for x_{pz}.

For different values of the applied reaction force P, Figure 6 shows the mode I cohesive traction profiles in the fracture process zone computed with the two approaches (FE with pre-defined interfaces and PU-FE). One can notice that good agreement is obtained also in this case.

In Figure 7 the results obtained with the symmetric and biased PU-FE meshes of

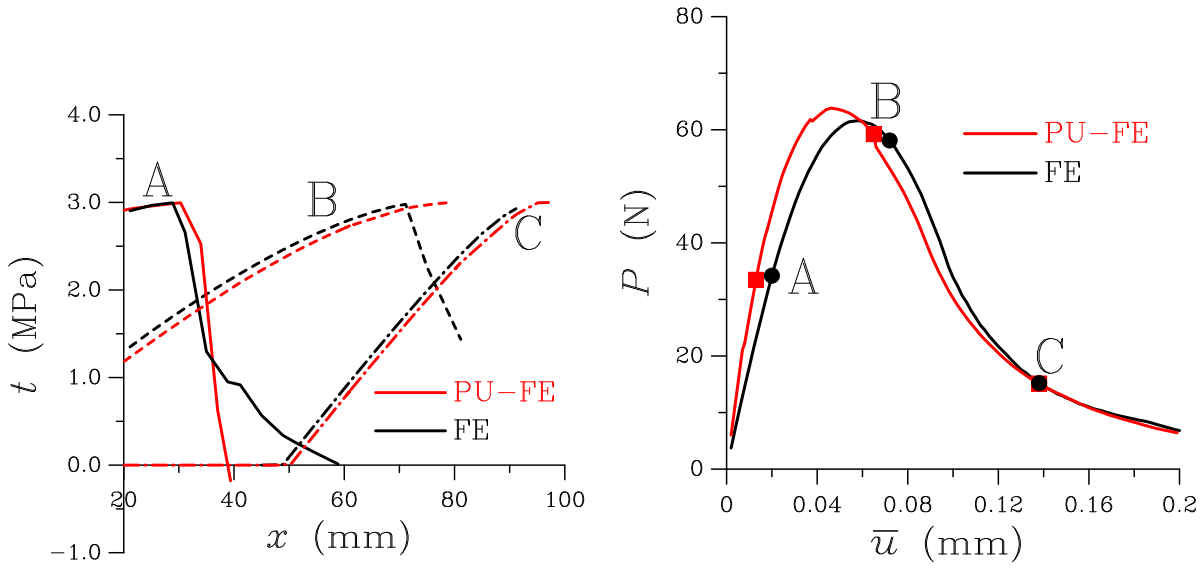

(a) (b)

Figure 6: (a) Mode I cohesive tractions in the fracture process zone at the three different stages of crack growth marked in (b).

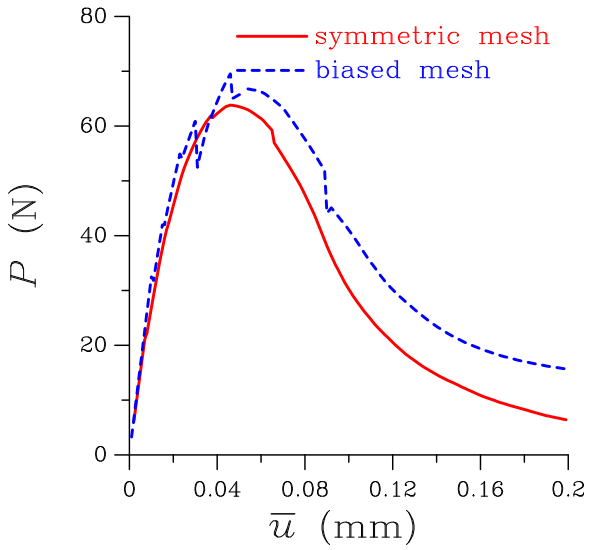

Figure 7: Effects of the mesh on the measured load P vs load point displacement $\bar{u}$ specimen response.

Figure 4 are compared. As expected, the different discretization affects the pre-peak $P-\bar{u}$ response only marginally, while a noticeable difference is evidenced in the softening branch. The higher reaction peak in the biased mesh is motivated by the fact that the resolved traction on an inclined crack is lower than the nominal applied one, while the longer zig-zag path followed by the propagating fracture implies a higher dissipation and therefore a larger fracture energy.

Acknowledgements

The financial support of MURST-Cofinancing Program 2000 and of LSC-Politecnico of Milan is gratefully acknowledged.

References

[1] I. Babuška, G. Caloz, and J. Osborn. Special finite element methods in a class of second order elliptic problems with rough coefficients. *SIAM Journal of Numerical Analysis*, 31:945–981, 1994.

[2] J.M. Melenk and I. Babuška. The partition of unity finite element method: basic theory and applications. *Computer Methods in Applied Mechanics and Engineering*, 139:289–314, 1996.

[3] G. Bolzon, G. Maier, and F. Tin-Loi. On multiplicity of solutions in quasi-brittle fracture computations. *Computational Mechanics*, 19:511–516, 1997.

[4] G. Bolzon and A. Corigliano. A discrete formulation for elastic solids with damaging interfaces. *Computer Methods in Applied Mechanics and Engineering*, 140:329–359, 1997.

[5] A. Pandolfi, P. Krysl, and M. Ortiz. Finite element simulation of ring expansion and fragmentation: The capturing of length and time scales through cohesive models of fracture. *International Journal of Fracture*, 95:1–18, 1999.

[6] M. Jirasek and T. Zimmerman. Embedded crack model: I. Basic formulation. *International Journal for Numerical Methods in Engineering*, 50:1269–1290, 2001.

[7] M. Jirasek and T. Zimmerman. Embedded crack model: II. Combination with smeared cracks. *International Journal for Numerical Methods in Engineering*, 50:1291–1305, 2001.

[8] G. Bolzon and A. Corigliano. Finite elements with embedded discontinuity: a generalised variable formulation. *International Journal for Numerical Methods in Engineering*, 49:1227–1266, 2000.

[9] G.N. Wells and L.J. Sluys. Three-dimensional embedded discontinuity model for brittle fracture. *International Journal of Solids and Structures*, 38:897–913, 2000.

[10] T. Strouboulis, K. Copps, and I. Babuška. The generalized finite element method. *Computer Methods in Applied Mechanics and Engineering*, 190:4081–4193, 2001.

[11] G.N. Wells and L.J. Sluys. A new method for modelling cohesive cracks using finite elements. *International Journal for Numerical Methods in Engineering*, 50:2667–2682, 2001.

[12] C.A. Duarte, I. Babuška, and J.T. Oden. Generalized finite element methods for three-dimensional structural mechanics problems. *Computers and Structures*, 77:215–232, 2000.

[13] N. Moës, J. Dolbow, and T. Belytschko. A finite element method for crack growth without remeshing. *International Journal for Numerical Methods in Engineering*, 46:131–150, 1999.

[14] N. Sukumar, N. Moës, B. Moran, and T. Belytschko. Extended finite element method for three-dimensional crack modeling. *International Journal for Numerical Methods in Engineering*, 48:1549–1570, 2000.

[15] C.A. Duarte, O.N. Hamzeh, T.J. Liszka, and W.W. Tworzydlo. A generalized finite element method for the simulation of three-dimensional crack propagation. *Computer Methods in Applied Mechanics and Engineering*, 190:2227–2262, 2001.

[16] G. Cocchetti, G. Maier, and X.P. Shen. Piecewise linear models for interfaces and mixed mode cohesive cracks. *To appear*, 2001.